



# Fabrication of cellulose carbamate hydrogel-dressing with rarasaponin surfactant for enhancing adsorption of silver nanoparticles and antibacterial activity

Vania Bundjaja<sup>a</sup>, Shella Permatasari Santoso<sup>c,a,\*</sup>, Artik Elisa Angkawijaya<sup>b,\*\*</sup>, Maria Yuliana<sup>c</sup>, Felycia Edi Soetaredjo<sup>c,a</sup>, Suryadi Ismadi<sup>c</sup>, Aning Ayucitra<sup>c</sup>, Chintya Gunarto<sup>a</sup>, Yi-Hsu Ju<sup>a,b,d</sup>, Ming-Hua Ho<sup>a</sup>

<sup>a</sup> Chemical Engineering Department, National Taiwan University of Science and Technology, #43, Sec. 4, Keelung Rd., Taipei 10607, Taiwan

<sup>b</sup> Graduate Institute of Applied Science and Technology, National Taiwan University of Science and Technology, #43, Sec. 4, Keelung Rd., Taipei 10607, Taiwan

<sup>c</sup> Department of Chemical Engineering, Widya Mandala Surabaya Catholic University, #37 Kalijudan Rd., Surabaya 60114, East Java, Indonesia

<sup>d</sup> Taiwan Building Technology Center, National Taiwan University of Science and Technology, #43, Sec. 4, Keelung Rd., Taipei 10607, Taiwan

## ARTICLE INFO

### Keywords:

Cellulose carbamate  
Silver nanoparticles  
Wound dressing  
Antibacterial dressing

## ABSTRACT

Bacterial contamination on external wounds is known to be a factor that prevents wound healing and triggers tissue damage. Hydrogel-dressings with antibacterial activity is a useful medical device to avoid this contamination, wherein the antibacterial activity can be provided via incorporation of silver nanoparticles (AgNPs). Contrary to the conventional two-step preparation of an AgNPs-loaded hydrogel (AgNPs@hydrogel), this work aims to establish a new and facile synthesis method employing the adsorption principle. Once AgNO<sub>3</sub> adsorbed into active sites of the hydrogels, in situ reductions using NaBH<sub>4</sub> was employed to produce AgNPs@hydrogel. The effect of surfactant addition on the AgNO<sub>3</sub> loading and the antibacterial activity of the resulting hydrogel dressing was investigated. The outcome of this work indicates that the addition of rarasaponin not only can increase the loading of AgNPs on cellulose carbamate hydrogel (CCH) but also significantly enhance the antibacterial activity of the resulted hydrogel-dressing. Superior to the other studied surfactant, the loading capacity (LC) of AgNPs is found to be 10.15, 9.94, and 7.53 mg/g for CCH modified with rarasaponin, CTAB, and Tween80, respectively. These findings conclude that the addition of surfactant, especially rarasaponin, can effectively improve the loading of AgNPs onto hydrogel-dressing via adsorption and promote the antibacterial activity. Furthermore, the cytotoxic test shows that the hydrogel-dressings have good biocompatibility toward skin fibroblast cells.

## 1. Introduction

The development of antibacterial dressing for the treatment of external wounds has received considerable interest in recent years. The urge for this development is particularly triggered by the emergence of diabetes-related diseases, such as foot ulceration [1]. The existence of antibacterial properties in the wound dressing is crucial to prevent further tissue damage due to bacterial contamination and infection; these properties can be established by grafting antibacterial agents. Broad-spectrum antibacterial agents are usually used in wound dressing; these agents have complex mechanisms in interacting with

bacterial cells, thereby avert the bacteria to develop resistance. Silver nanoparticles (AgNPs) are known as a powerful broad-spectrum antimicrobial agent which have a long-lasting antimicrobial effect against various strains of bacteria and drug-resistant pathogens [2–7]. For centuries, AgNPs have been used to generate antimicrobial activity of different wound healing materials or devices, such as wound dressing, antiseptics, and medical devices [8].

Numerous techniques have been established to synthesis AgNPs, such as chemical reduction, photochemical, electrochemical, irradiation, thermal, biological, and microemulsion [9–18]. Among them, the chemical reduction is the most frequently adopted method owing to its

\* Correspondence to: S. P. Santoso, Department of Chemical Engineering, Widya Mandala Surabaya Catholic University, #37 Kalijudan Rd., Surabaya 60114, East Java, Indonesia. Chemical Engineering Department, National Taiwan University of Science and Technology, #43, Sec. 4, Keelung Rd., Taipei 10607, Taiwan.

\*\* Corresponding author.

E-mail addresses: [sella\\_p5@yahoo.com](mailto:sella_p5@yahoo.com) (S.P. Santoso), [artikelisa@mail.ntust.edu.tw](mailto:artikelisa@mail.ntust.edu.tw) (A.E. Angkawijaya).

<https://doi.org/10.1016/j.msec.2020.111542>

Received 15 April 2020; Received in revised form 7 September 2020; Accepted 19 September 2020

Available online 23 September 2020

0928-4931/ © 2020 Elsevier B.V. All rights reserved.

concise and straightforward approach [19]. The tendency of AgNPs to form aggregates is a persistent problem in its synthesis, where the formation of aggregates can diminish the antibacterial efficiency of AgNPs [20]. Integration of AgNPs into supporting matrixes or polymeric material (like clay minerals, alginate-based hydrogel, chitosan, cellulose, collagen, PVA-PVP, and HEMA-PEGDA) is reportedly preventing the formation of the aggregates [21–31]. Hydrogels have gained much interest among these supporting materials, owing to their superior medical biocompatibility and immense water retention ability. Furthermore, hydrogels also can be directly applied as wound dressing materials [32,33].

Various natural and synthetic polymeric materials are widely available for preparing hydrogels, such as cellulose. In addition to the natural availability of cellulose, the beneficial biological properties of cellulose also promote its potency as raw material for wound dressing hydrogels. The beneficial biological properties of cellulose are including non-toxic, biodegradable, and high similarity in mechanical properties to natural tissue [34]. The biocompatibility and antimicrobial activity of cellulose in the form of hydrogel have been proven [35,36]. Herein, cellulose is utilized as the raw material for preparing hydrogel and also as a template for AgNPs nano-formulations. This combination can be a promising approach to prevent AgNPs aggregation while producing antimicrobial dressing.

The preparation of cellulose hydrogel involves two main steps, that is the dissolution of the cellulose chain and the formation of a three-dimensional network via cross-linking. The nature of cellulose, which is not soluble in water, is a challenge in preparing cellulose-based hydrogels. Various dissolution methods have been established to resolve this limitation, such as the viscose process, carbamation, lyocell process, and the use of the ionic-liquid system [37]. Carbamation of cellulose to produce cellulose derivatives (i.e., cellulose carbamate) is known as an environmental dissolution method of cellulose compared to another soluble cellulose derivative (i.e., cellulose xanthogenate) which the synthesis accompanied by the generation of hazardous by-products. Cellulose carbamate (CC) has better solubility in alkaline and organic solution compared to cellulose [38]. Furthermore, CC reported to possess bacteriostatic properties, which make it more resistant against microbial contamination and enzymatic-cleavage compare to cellulose. Gan et al. also reported that CC-based hydrogel has an enhanced porosity compare to cellulose hydrogels [39]. Therefore, in this work, the carbamation process was chosen to dissolve the cellulose.

A new-facile approach in the incorporation of AgNPs to hydrogel was introduced. That is, by employing adsorption techniques of  $\text{Ag}^+$  ions onto the surface active sites of the hydrogel, followed by in situ reductions of the attached  $\text{Ag}^+$  ions. This approach allows the binding of large numbers of AgNP to the surface of the hydrogel dressing, thereby enhancing the antibacterial activity against the target bacteria. Furthermore, this approach could be an improvement over the conventional AgNPs hydrogel-dressing—wherein, in the preparation, AgNPs are integrated into the hydrogel matrix. So, the effectiveness of AgNPs in the center of the hydrogel matrix is reduced due to the difficulty of reaching the target bacteria.

The effect of surfactant addition in improving the AgNPs loading capacity of the hydrogel was assessed in this work, where this case is yet to be significantly studied. The addition of surfactants also can enhance antibacterial properties. As reported by Cuahtecontzi-Delint et al., the incorporation of non-ionic surfactants (Triton X-100, Polyvinyl Pyrrolidone, and Tween80) on  $\text{CeO}_2$  nanoparticles can enhance the antibacterial activity of the material [40]. An in vivo study by Sibbald et al. showed that a polymeric membrane foam pad filled with surfactant could overcome bacterial damage and facilitate wound closure [41]. Additionally, surfactant supplementation may significantly improve the stability of AgNPs [42,43]. The effect of three surfactants on the loading of AgNPs to CC-based hydrogel was assessed in this work. The surfactants used are (1) the non-ionic Tween80, (2) cationic CTAB, and (3) rarasaponin, which had no formal charge, but were

deacylated when dissolved in polar solvents to negatively charged surfactants [44].

So far, there are still no studies that examine the effect of adding surfactants, especially rarasaponin, to increase the loading of AgNPs in CC-hydrogel (AgNPs@CCH). This work aims to investigate the effect of surfactants (especially rarasaponin) in the loading capacity of AgNPs to CCH. Some physicochemical measurements were carried out to characterize the material. The evaluation of cytotoxicity was carried out quantitatively using MTT assay. Hereinafter, the antibacterial activity of AgNPs@CCH with and without surfactant modification was investigated against *Escherichia coli* (gram-negative bacteria) and *Staphylococcus aureus* (gram-positive bacteria).

## 2. Materials and methods

### 2.1. Materials

Laboratory filter paper (Whatman #1) was used as a source of cellulose fibers. The following chemicals were used in this experiment: urea ( $\text{CO}(\text{NH}_2)_2$ , 98%; EMD Millipore, Darmstadt, Germany), sodium hydroxide (NaOH, 96%; EMD Millipore, Darmstadt, Germany), epichlorohydrin (ECH,  $\geq 99\%$ ; Sigma-Aldrich, Singapore), silver nitrate ( $\text{AgNO}_3$ ;  $\geq 99.8\%$ ; Spectrum Chemical, Gardena, California), and sodium borohydride ( $\text{NaBH}_4$ , 99%; Sigma-Aldrich, Steinheim, Germany). The following surfactants were used for modification: polyoxyethylene sorbitan monooleate (Tween80; non-ionic surfactant; EMD Millipore, Darmstadt, Germany) cetyltrimethylammonium bromide (CTAB, cationic surfactant;  $> 98\%$ ; Sigma-Aldrich, Darmstadt, Germany), and *Sapindus rarak DC* fruit extract (rarasaponin; anionic surfactant; *Sapindus rarak DC* fruit obtained from Malang, East Java, Indonesia). The structural properties and critical micelle concentration (CMC) of surfactants were presented in Supplementary Material Table S1. Rarasaponin was extracted from *Sapindus rarak* according to the previously published work [44], with a slight modification that is ethanol was used as the solvent instead of water. All solutions were prepared using reverse osmosis water obtained from Kusatsu water purification equipment with  $8.3 \mu\text{S}/\text{cm}$  conductivity at  $28.5^\circ\text{C}$ .

### 2.2. Carbamation of cellulose

The filter paper was cut into small pieces and pulp by soaking 1 g of filter paper in 100 mL of 3% NaOH solution for 1 h, with constant stirring at room temperature. The pulp was washed with reverse osmosis (RO) water until the washing solution pH reduces to 6. The pulp was then dried in a  $60^\circ\text{C}$  oven overnight. The carbamation process was carried out by soaking 1 g of dry pulp in 20 mL of urea solution at a ratio of cellulose to urea of 1:1, 1:3, and 1:5. The mixture was stirred vigorously and then heated in an autoclave at  $160^\circ\text{C}$ . After 1 h, the carbamation reaction was quenched by immersing the autoclave in a water bath filled with ice water. The resulting cellulose carbamate (CC) was washed several times with RO water to remove excess urea. Then, CC is dried in the oven overnight and stored in a desiccator. The resulting CC is coded as CC1, CC3, and CC5 according to the cellulose to urea ratio.

### 2.3. Preparation of CC hydrogel

The alkaline solution was prepared by combining 7 wt% NaOH and 12 wt% urea, and then precooled at  $-13^\circ\text{C}$ . Into 100 g of the precooled solution, 4 wt% of CC was added and stirred until a transparent-viscous solution formed. The viscous solution was then centrifuged at 5000 rpm for 3 min to remove trapped air bubbles. Then, 5% (w/v) of ECH was added dropwise and stirred for 20 min. The gel solution was cast into a multi-well plate and allowed to stand for about 15 min to condense the gel. The consolidation of the gel was initiated by heating at  $60^\circ\text{C}$  in a water bath. The resulting hydrogel was continuously washed in flowing RO water for 2 d.

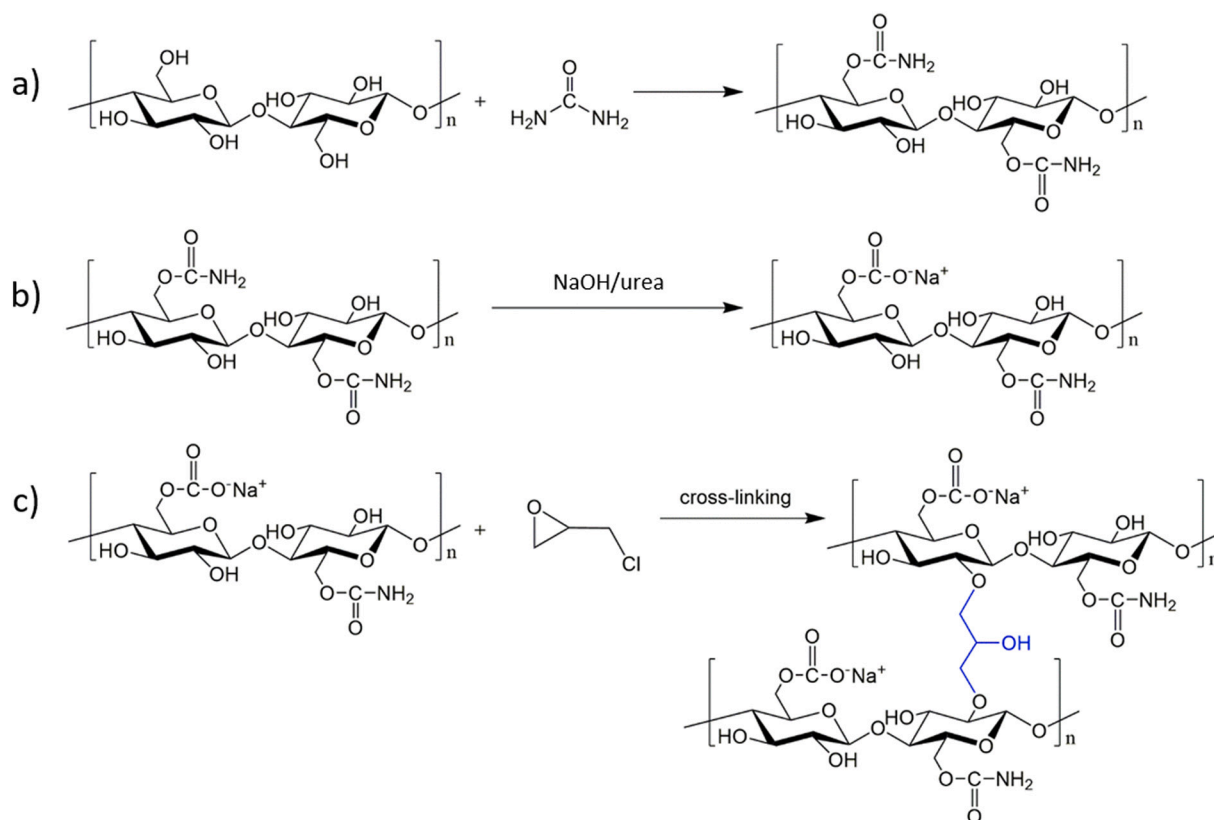


**Fig. 1.** Schematic diagram of the process of (a) cellulose carbamation, (b) dissolution of cellulose carbamate in NaOH/urea, and (c) cross-linking of cellulose carbamate with ECH.

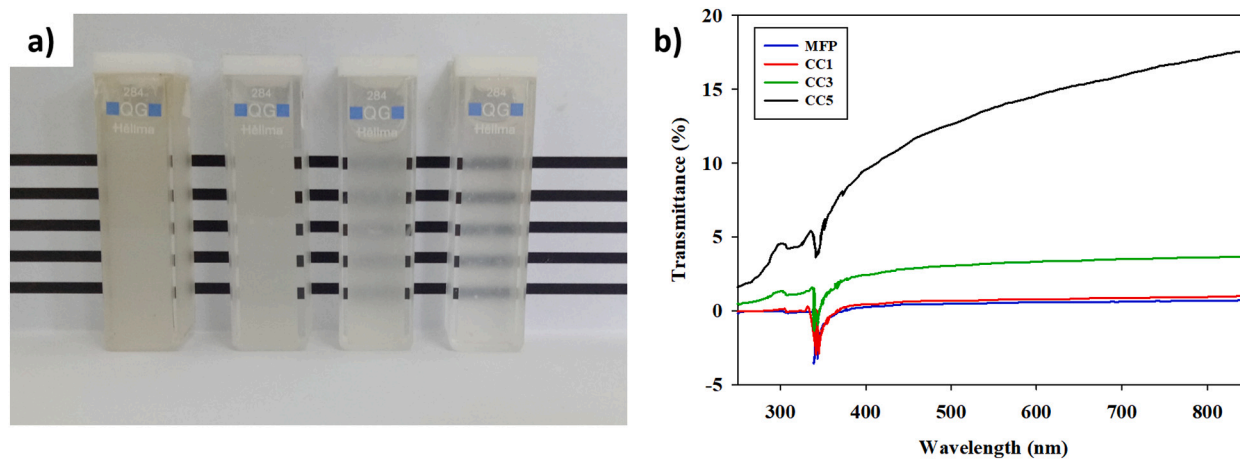


**Fig. 2.** Optical properties of CCH (a) digital photos that show the level of transparency, from left to right: MFP, CC1, CC3, and CC5, and (b) UV-Vis transmittance spectrum.

**Table 1**  
Effect of surfactant on  $\text{pH}_{\text{pzc}}$  of CCH.

Modifying surfactant	Surfactant conc. (mM)	Sample code	$\text{pH}_{\text{pzc}}$
–	–	CCH	6.18
Tween80	5	CCH-T5	6.45
	10	CCH-T10	6.34
CTAB	5	CCH-C5	7.78
	10	CCH-C10	8.03
Rarasaponin	5	CCH-R5	5.54
	10	CCH-R10	5.25

#### 2.4. Modification of CC hydrogel using surfactants

Rarasaponin, Tween80, and CTAB are used as surfactants to modify CC hydrogel (CCH). Briefly, 10 mL of surfactant at a concentration of 5 or 10 mM was prepared in distilled water. The freeze-dried hydrogel disk (10 mm diameter, 2 mm height, and dry weight  $\pm 10$  mg) was then soaked in the surfactant solution for 48 h at room temperature. The hydrogel was then rinsed with RO water and then dried using a freeze-dryer. The surfactant modified hydrogels were denoted as CCH-x, with  $x = \text{T}, \text{C},$  or  $\text{R}$  according to the type of surfactant Tween80, CTAB, and rarasaponin, respectively.

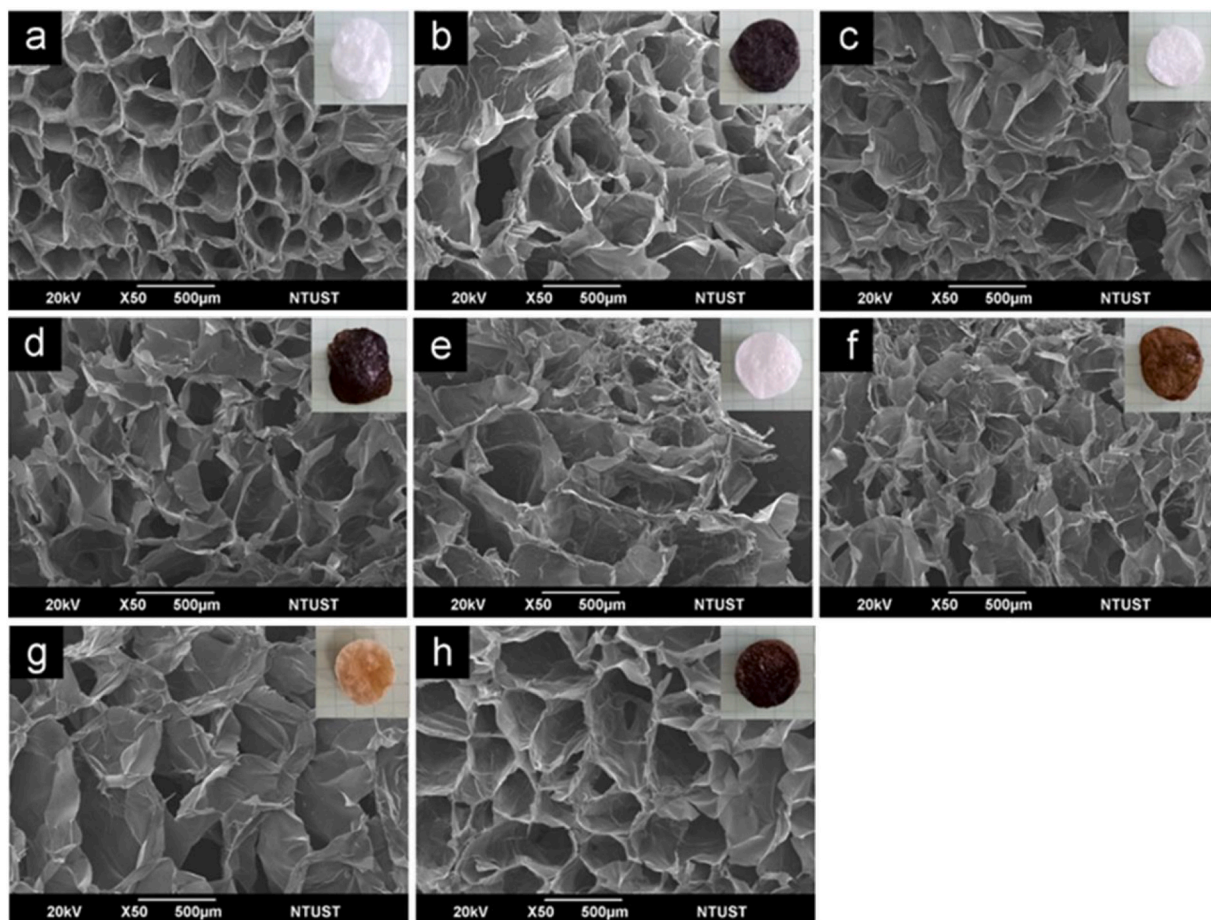


Fig. 3. SEM images AgNPs-loaded (a–b) CCH, (c–d) CCH-T, (e–f) CCH-C, and (g–h) CCH-R. The insets in panels show the physical appearance of hydrogels after drying. (For interpretation of the references to color in this figure, the reader is referred to the web version of this article.)

### 2.5. AgNPs embedding into CCH

The formation of AgNPs was carried out using chemical reduction techniques with  $\text{NaBH}_4$  as its reducing agent [45]. Hydrogel discs (with or without surfactant modification) were immersed in 10 mL of 10 mM  $\text{AgNO}_3$  solution. After 24 h immersion, the  $\text{Ag}^+$ -containing hydrogels were transferred into 10 mL of 10 mM  $\text{NaBH}_4$  solution and left for 2 h. The obtained AgNPs-loaded CCH was washed using RO water and subsequently dried using a freeze-dryer. The concentration of embedded  $\text{Ag}^+$  ions was measured using an atomic absorption spectrophotometer (AAS) against  $\text{AgNO}_3$  in 0.5 M  $\text{HNO}_3$  as the standard.

### 2.6. Characterization and analysis

#### 2.6.1. Characterizations

Transparency measurement of CCH was carried out by pouring the gel into a quartz cuvette with a 10 mm pathlength. Then the transmittance spectra were recorded using UV–Vis Spectrophotometer (Shimadzu UV-1700) at 850–250 nm wavelength with 400 nm/min scanning speed. The cross-sectional images and subsequent elemental diagram of the samples were taken using a field-emission scanning electron microscope (JEOL JSM-6390) with an attachment of energy dispersive spectroscopy (EDS) analyzer; images were taken at an accelerating voltage of 20 kV. Before SEM imaging, samples were freeze-dried and plunged into liquid nitrogen. The samples were then broken into small fractures; fractures were then coated with platinum by a fine auto coater (JEC-3000FC). The morphology of AgNPs in the hydrogels was observed by the use of FEI Tecnai G2 TF20 Super TWIN. The TEM specimens were prepared by crushing the samples and dispersing in

ethanol. Sample solutions were deposited on a carbon-coated copper grid and allowed to sit to evaporate the solvent prior to the imaging. The dimension of AgNPs from TEM micrographs was measured using ImageJ 1.52a software. Surface functional groups were characterized using Fourier transformed infrared (FTIR) spectra. The FTIR pattern was accumulated from 20 scans using a Shimadzu 8400S spectrophotometer equipped with a KBr beam splitter in 4000–400  $\text{cm}^{-1}$  region. The crystal diffraction pattern was recorded by Bruker D2 Phaser X-ray diffractometer with a monochromatic high-intensity  $\text{Cu K}\alpha$  radiation operating at 30 kV and 10 mA.

#### 2.6.2. Surface charge measurement ( $\text{pH}_{\text{pzc}}$ )

The  $\text{pH}_{\text{pzc}}$  analysis was performed as described by Orfao et al. (2006), with minor modifications [46]. A series of capped Erlenmeyer flask containing 10 mL NaCl solution (0.01 M) were prepared. Each flask was adjusted to a specific pH, at a pH range of 2 to 10, by the addition of HCl and NaOH. To each flask, a 30 mg sample was added. The sample was immersed for 48 h with constant shaking at 100 rpm and a constant temperature of 30 °C. The final pH of each solution was measured using a pH meter (Mettler-Toledo S20 SevenEasy). The  $\text{pH}_{\text{final}}$  versus  $\text{pH}_{\text{initial}}$  values were plotted, the corresponding intersection point of these two curves (at  $\text{pH}_{\text{final}} = \text{pH}_{\text{initial}}$ ) was identified as  $\text{pH}_{\text{pzc}}$ .

#### 2.6.3. Measurement of loaded AgNPs

The amount of Ag loading on CCH was measured using atomic absorption spectrophotometric (AAS) (Shimadzu AA-6200) equipped with an autosampler, silver hollow cathode lamp, and air-acetylene flame. The AgNPs-hydrogel discs were first dissolved in 5 mL of aqua regia (prepared by mixing HCl and  $\text{HNO}_3$  solution at ratio 3:1 (v/v)). The

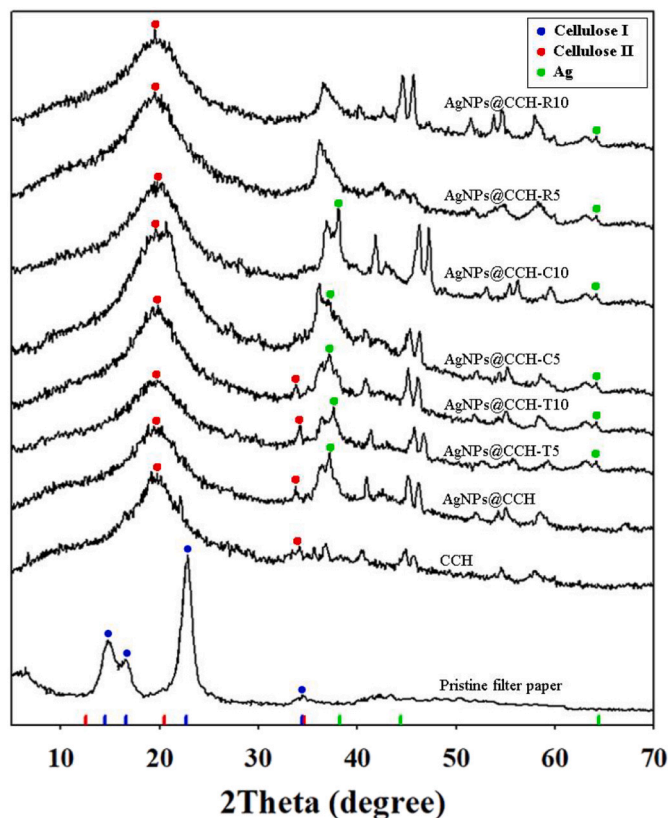


Fig. 4. (a) X-ray diffraction (XRD) pattern of pristine filter paper, AgNPs@CCH, and surfactant modified AgNPs@CCH. (b) SAED pattern of AgNPs@CCH-R10.

AgNPs loading capacity (LC) of the hydrogel is calculated using the following formula:

$$LC (\mu\text{g AgNP/mg dry hydrogel}) = \frac{C \times V}{m - (LC \times m)}$$

where C ( $\mu\text{g/mL}$ ) is the amount of AgNPs in the solution, V (mL) is the volume of the solution, and m (mg) is the mass of dry hydrogel along with the loaded AgNP. The divider on the right needs to be subtracted by the loaded-AgNPs weight, leaving only dry hydrogel mass (without AgNPs). A goal-seek function in Microsoft Excel was used to solve the LC mass balance.

#### 2.6.4. Deformability measurement

Penetrometer (Ashoka Enterprises) was employed to measure the deformability of swollen hydrogels at 30 °C. A needle with an attached load of 50 g with a square-shaped ends precisely adjusted to touch the surface of the cylindrical hydrogel (10 mm in diameter, 2 mm in height). Then, the needle was allowed to sink into the sample for 5 s. The values shown on the scale were recorded, and the deformability was expressed in mm/g s.

#### 2.6.5. Cytotoxicity assay

The cytotoxicity of hydrogel samples was evaluated in vitro toward the skin fibroblast, L929 cell, by 3-(4,5-dimethylthiazol-2-yl)-2,5-diphenyltetrazolium bromide (MTT) assay. Dulbecco's modified eagle's medium (DMEM) was used as the culture media. Cells were seeded as a monolayer in culture flasks at 37 °C  $\pm$  1 °C, 90%  $\pm$  10% humidity, and 5.0%  $\pm$  1.0% CO<sub>2</sub>/air. After 24 h of incubation, the medium was substituted with a serum-free medium containing prepared hydrogel extract (0.2 g hydrogel in 1 mL medium) according to ISO 10993-5 and then incubated for 24 h at 37 °C. Following, 5 mg/mL of MTT was added and incubated for a further 4 h. After removing the medium, DMSO was added and shaken for 30 min. The absorbance of the purple

formazan crystals was recorded at 570 nm using an automatic microplate reader (ELx800; Bio-Tek Instruments, Winooski, VT, USA).

#### 2.6.6. Antibacterial activity assay

The disk diffusion method was applied to assay the antibacterial activity of hydrogel samples. The inhibitory effect of the samples was tested against two bacterial strains, that is *Escherichia coli* (*E. coli*, ATCC 25922; gram-negative) and *Staphylococcus aureus* (*S. aureus*, ATCC 25923; gram-positive). Before the assay, bacterial suspension at a concentration of 10<sup>8</sup> CFU/mL was prepared according to the 0.5 McFarland standard. The bacterial suspension was then inoculated onto Mueller-Hinton agar plates using a sterile cotton swab. The freeze-dried AgNP-hydrogel samples were pressed into discs with a diameter of 10 mm. The pressed hydrogel discs were placed on the surface of the agar plates aseptically. The inhibition zone was measured after 24 h incubation at 37 °C. Ampicillin (10  $\mu\text{g}$ ) and AgNP-free hydrogels were used as a positive and negative control, respectively.

### 3. Results and discussion

The AgNPs-loaded cellulose carbamate hydrogel (CCH) was denoted as AgNPs@CCH. The Tween80, CTAB, and rarasaponin modified AgNPs@CCH samples were denoted as AgNPs@CCH-T, AgNPs@CCH-C, AgNPs@CCH-R, respectively.

#### 3.1. Carbamation of cellulose and CCH formation mechanism

Hydrothermal carbamation of cellulose occurs through the substitution of functional groups; schematically, the carbamation is illustrated in Fig. 1a. Urea functional groups, specifically carbonyl (C=O) and amine groups (NH<sub>2</sub>), were substituted with primary alcohol groups (-OH, at the sixth position) of cellulose [39,47]. In the carbamation process, the level of urea dose affects the transparency of the hydrogel. A high dose of urea resulting in the hydrogel with high transparency, where the transparency order is mercerized filter paper (MFP)  $\leq$  CC1 < CC3 < CC5 (most transparent). The degree of transparency of the hydrogel can be observed from the ability of the hydrogel to transmit light. Based on the results in Fig. 2b, MFP and CC1 transmissions are close to zero, indicating a lack of cellulose distribution, thus blocking light transmission.

Meanwhile, CC3 and CC5 samples (with higher carbamation levels) showed a high light transmission; this indicates proper dissolution and distribution of cellulose. High carbamation levels cause weakening of hydrogen bonds between cellulose chains so that the dissolution is better. It was found that CC5, with the ratio of cellulose to urea 1:5, has the best transparency with a degree of substitution of  $0.34 \pm 0.03$  as calculated using the published equation [48] so that this ratio was chosen for further studies.

The formation of cellulose hydrogel (without the carbamation process) has been widely reported, where the success of hydrogel formation depends on the process of cellulose dissolution [49,50]. The mechanism of the formation of CCH is similar to the formation of cellulose hydrogels, where its formation begins with the dissolution of CC in NaOH/urea solution (Fig. 1b). Next, the dissolved CC chain is cross-linked into a three-dimensional network with the help of ECH, as illustrated in Fig. 1c. The cross-linking process begins with the opening of the ECH epoxide ring through a nucleophilic attack; a basic pH condition is required in this process. Then the opened ECH ring interacts with the hydroxyl group of cellulose, which then forms interconnected networks [51–54].

#### 3.2. Characterization of the hydrogels

The effect of surfactant addition on the surface charge (without the addition of AgNPs) was investigated through its p*H*<sub>pzc</sub> value. The plot showing p*H*<sub>pzc</sub> is shown in Fig. S1 and the values are recorded in

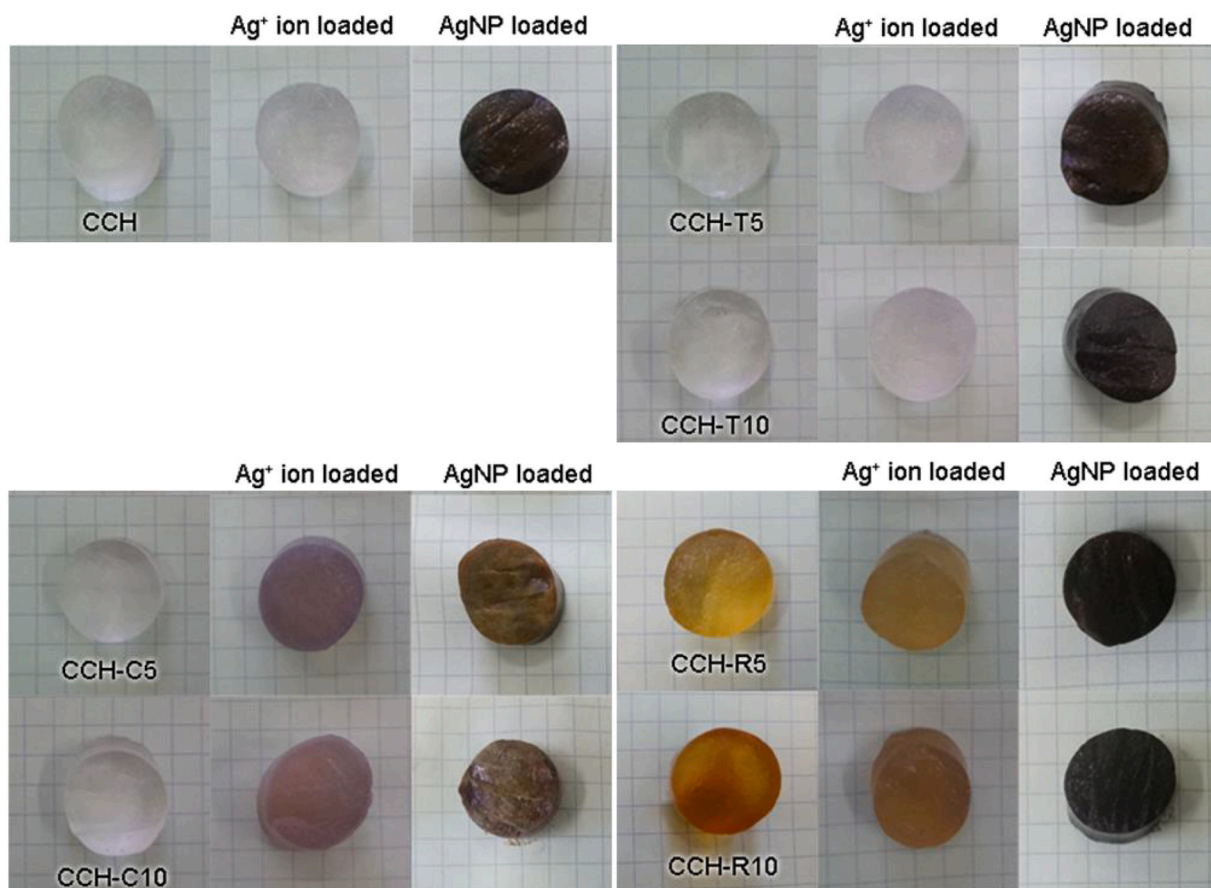


**Fig. 5.** The physical appearance of hydrogels in its swelling stage. (For interpretation of the references to color in this figure, the reader is referred to the web version of this article.)

**Table 1.** Modifications using cationic surfactant (CTAB) give high  $\text{pH}_{\text{pzc}}$  values. This is because the positively charged surfactant makes the CCH surface charge more positive so that more negative ions are needed to neutralize. In contrast, the  $\text{pH}_{\text{pzc}}$  value was lower for samples that were modified with anionic surfactants (rarasaponin). For CCH modified by a non-ionic surfactant (Tween80), the  $\text{pH}_{\text{pzc}}$  value did not show a significant difference to CCH.

The FTIR spectra are presented in Fig. S2, FTIR measurements were carried out on materials without AgNPs-loaded. The peak at wavenumber  $1700\text{ cm}^{-1}$  was observed in the CCH spectra (before and after modification with surfactants); this peak does not appear in the MFP sample. This peak corresponds to the stretching vibration of the carbonyl urethane-based group ( $\text{C}=\text{O}$ ), where it arises because of cellulose carbamation. The reduction in the intensity of the hydroxyl group ( $-\text{OH}$ ) at wavenumber  $3300\text{ cm}^{-1}$  was observed in CCH; this is caused by the reaction of urea with the cellulose  $-\text{OH}$  group as proposed in the mechanism of Fig. 1a [55].

Modification of CCH using different types of surfactants shows slightly different FTIR spectra. Interaction between surfactants with active groups on CCH is triggered by hydrophobic interactions that occur between hydrophobic surfactant tails and hydrophobic cellulose sites, and also hydrophilic interactions between surfactant micelles and hydrophilic cellulose groups [56,57]. In CCH-T, the peak corresponding to  $\text{C}=\text{O}$  stretch at  $1718\text{ cm}^{-1}$ , asymmetric  $\text{CH}_2$  stretch at  $2920\text{ cm}^{-1}$ , and symmetrical  $\text{CH}_2$  stretch at  $2869\text{ cm}^{-1}$  can be observed. In CCH-C, the following peaks are found,  $\text{C}=\text{O}$  stretch at  $2915$ ,  $2857$  and  $1701\text{ cm}^{-1}$ ; tertiary amine  $[\text{RN}(\text{CH}_3)_3^+]$  stretch at  $903\text{ cm}^{-1}$ ; and  $-(\text{CH}_2)-$  in-plane swing at  $720\text{ cm}^{-1}$ . In CCH-R,  $\text{C}=\text{C}$  stretch was observed at  $1689\text{ cm}^{-1}$ .

SEM images for AgNPs-loaded CCH and surfactant-modified CCH are illustrated in Fig. 3. The morphology of the cross-section of the

hydrogel shows a spongiform structure with a pore diameter of around  $200\text{--}500\text{ }\mu\text{m}$ , and these pores facilitate space to retain water and AgNPs. The addition of surfactants and the reduction of  $\text{Ag}^+$  ions did not induce a significant change in the structural morphology of CCH. The presence of AgNPs on the CCH matrix was confirmed using EDX spectra (Fig. S3). All EDX spectra of the sample showed the peak of Ag; it was also seen that CCH, which was modified with surfactants, had higher Ag content.

The XRD pattern for the samples is presented in Fig. 4. Diffraction peak with a high intensity, which indicates the presence of cellulose I was observed for the MFP sample. Whereas for CCH, this peak is disappeared. Instead, diffraction peaks associated with cellulose II were found in CCH samples. As stated by Aleshina et al., the dissolution of cellulose causes damage to the crystalline structure of cellulose; thus, the peak of cellulose I disappear [58]. The XRD spectra of AgNPs@CCH-R, AgNPs@CCH-T, and AgNPs@CCH-C show peaks at  $2\theta=38.24^\circ$  and  $64.44^\circ$ , corresponds to (111) and (220) planes of face-centered cubic silver (JCPDS No. 04-0783); which also supported from SAED pattern, especially for AgNPs@CCH-R in inset Fig. 7d. Meanwhile, for AgNPs@CCH with no surfactant, the peak at  $2\theta = 64.44^\circ$  does not present; this is due to low AgNPs content. The alteration of the XRD pattern at  $2\theta = 38.24^\circ$  for both rarasaponin modified samples (AgNPs@CCH-R5 and AgNPs@CCH-R10) indicates that the presence of rarasaponin disrupts the crystalline structure of AgNPs.

### 3.3. Effect of surfactant on AgNPs loading

AgNPs are implanted into CCH by first soaking CCH in the  $\text{AgNO}_3$  salt solution.  $\text{Ag}^+$  reduction is then initiated using  $\text{NaBH}_4$  as a reducing agent, and thus, AgNPs are formed. The attachment of  $\text{Ag}^+$  ions to CCH is facilitated by the  $-\text{OH}$  group of CCH, which acts as anchor sites [59];

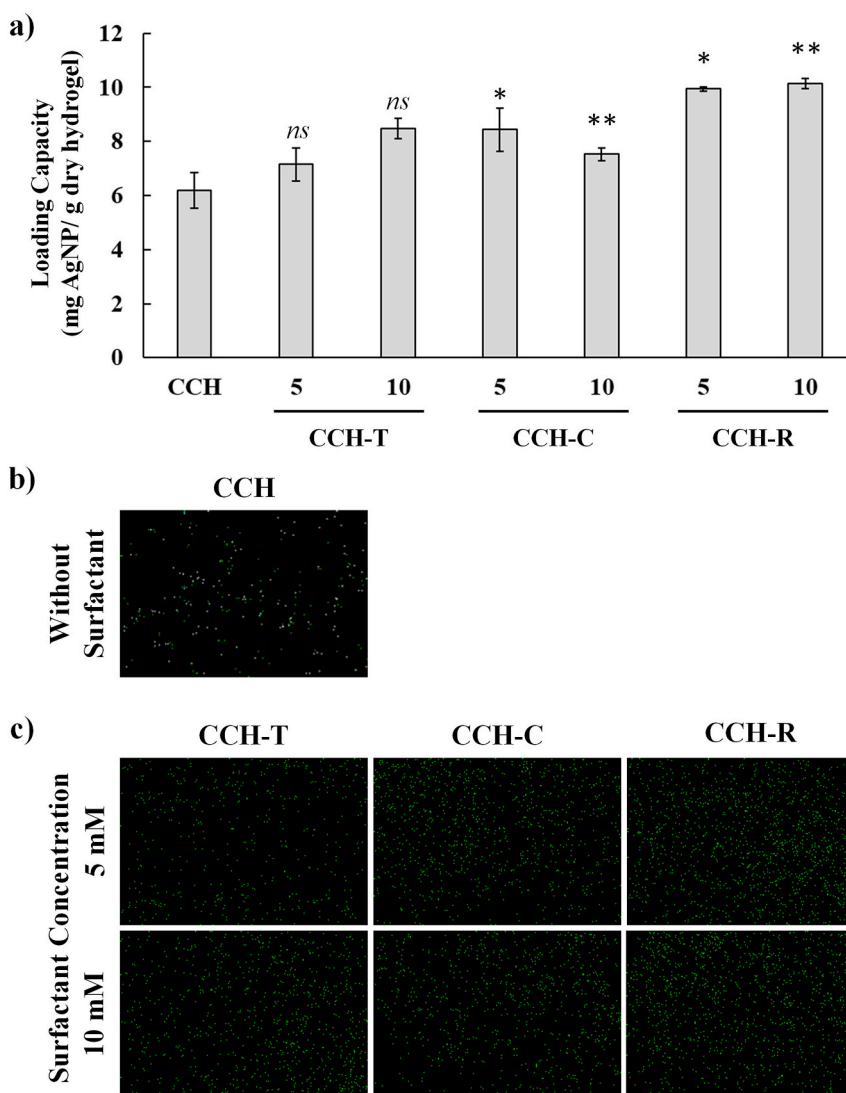


**Fig. 6.** (a) AgNPs loading on CCH, CCH-T, CCH-C, and CCH-R. Data are mean  $\pm$  SD from 2 replicates. Asterisks indicate statistical significance in comparison to CCH examined by Student's *t*-test; (\*\*, P value < 0.01; \*, P value < 0.05; ns, not significant)—All data show uncertainty < 5%. Elemental maps of Ag on (b) CCH and (c) surfactant-modified CCH.

this interaction is reinforced by electrostatic forces [45]. Also, the cross-linked networks provide free space that allows  $\text{Ag}^+$  to be anchored [60]. No morphological changes were observed for  $\text{Ag}^+$ -loaded CCH. However, visual changes can be observed, where the loading of AgNPs in CCH-C causes the color to turn purple (Fig. 5). This discoloration is caused by the formation of complexes between the  $\text{Ag}^+$  and the head group of CTAB [61]. Liu et al. also reported that  $\text{Ag}^+$  has a strong tendency to react with  $\text{Br}^-$  of CTAB; this is because  $\text{N}^+$  in the head group of CTAB cannot provide electron pairs to bind  $\text{Ag}^+$  [62].

The deposition of AgNPs in the hydrogel matrix can be visually confirmed by changing the color to blackish brown after reduction with  $\text{NaBH}_4$  [63], as shown in insets Figs. 3, and 5. To measure the amount of AgNPs contained in the hydrogel, AAS measurements were carried out in addition to the EDX analysis. Before the measurement of AAS, the AgNPs-loaded hydrogels were dissolved using aqua regia. AgNPs which are released into the solution is then measured; the results of the AAS measurement are shown in Fig. 6a. It can be seen that the addition and type of surfactant result in different Ag loading capacity (LC).

CCH, which is modified with the surfactant, has a higher LC value than unmodified CCH. The type of surfactant was also seen to affect LC values; modifications with Tween80 and CTAB gave lower LC values compared to rarasaponin. This is due to the anionic nature of

rarasaponin, which facilitates stronger electrostatic interactions with  $\text{Ag}^+$ . In addition, there is a probability that high surfactant concentrations (above critical micelle concentrations) allow the formation of micelles with the hydrophilic head facing out [64], and thus, create more sites to bind  $\text{Ag}^+$ . The lower LC in CCH modified by CTAB is due to the presence of  $\text{Br}^-$  in solution, significantly since  $\text{Br}^-$  can drag out  $\text{Ag}^+$  ions from the hydrogel matrix. Also, cationic CTAB also causes a more favorable surface charge of CCH. Thus  $\text{Ag}^+$  binding was hindered. In contrast, the addition of nonionic surfactant Tween80 did not affect the CCH surface charge.

Once adsorbed, the  $\text{Ag}^+$  ions bind with the  $-\text{OH}$  groups in the CCH matrix and surfactant micelles. These bounded  $\text{Ag}^+$  was reduced by the  $\text{NaBH}_4$  that penetrates hydrogel then form AgNPs with retained interaction toward the  $-\text{OH}$  groups of CCH [65] and also with the surfactant in the modified CCH matrix. The distribution of AgNPs in the hydrogel was investigated through mapping the silver element, as shown in Fig. 6b and c. It can be seen that AgNP is well dispersed in the hydrogel matrix, and also that more AgNP is observed to be distributed in surfactant-modified CCH.

The effect of surfactant on the morphology of AgNPs has been characterized. As seen in the TEM image in Fig. 7, the resultant AgNPs exhibit spherical nano-size. The histogram depicts the particle size distribution of

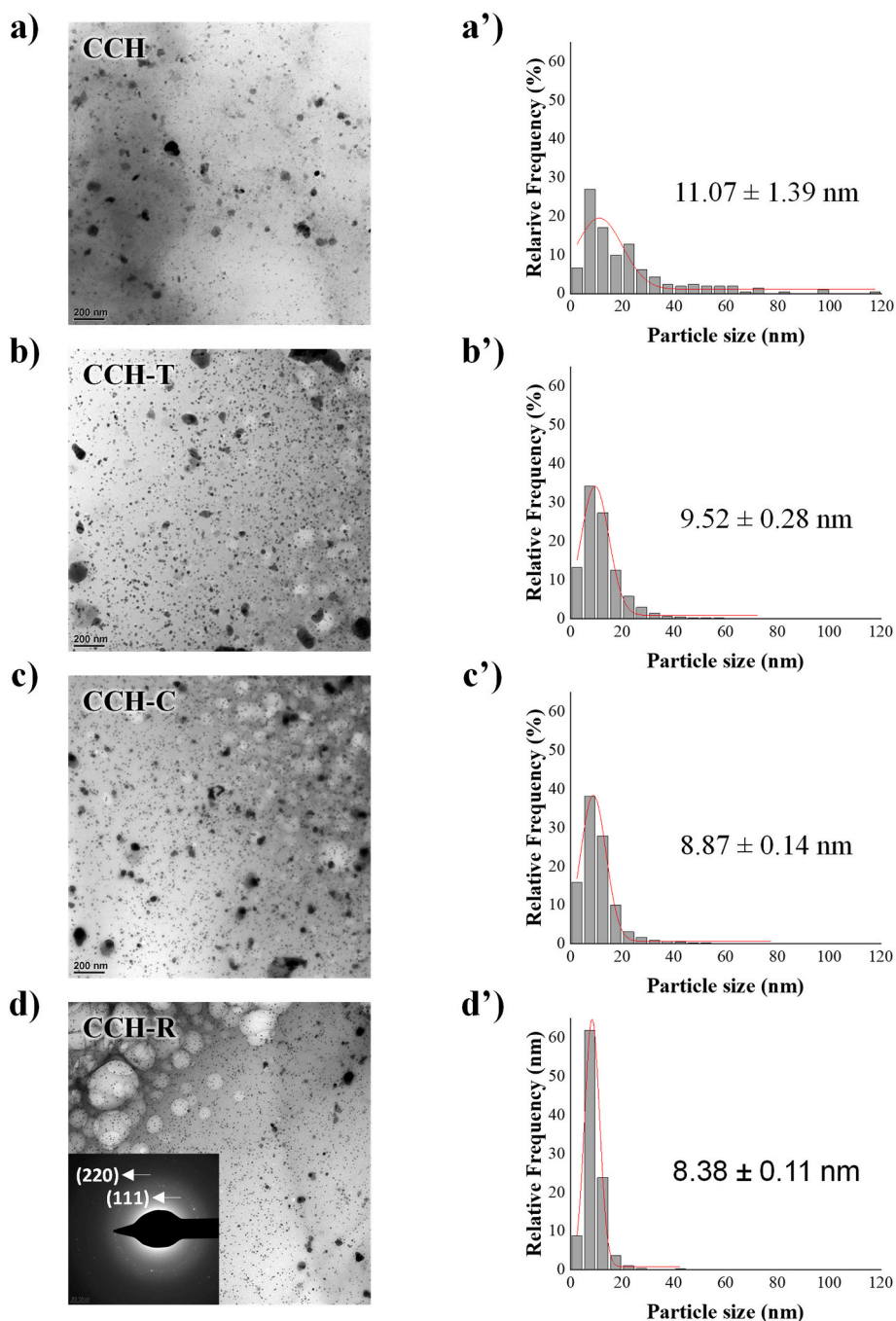


Fig. 7. TEM images and the corresponding histograms of the particle size distribution of AgNPs on (a, a') CCH, (b, b') CCH-T, (c, c') CCH-C, (d, d') CCH-R. The inset figure shows the SAED pattern of AgNPs@CCH-R.

the synthesized AgNPs@CCH with and without surfactant modification with a mean particle diameter of  $11.07 \pm 1.39$ ,  $9.52 \pm 0.28$ ,  $8.87 \pm 0.14$ , and  $8.38 \pm 0.11$  for CCH, CCH-T, CCH-C, and CCH-R, respectively. The AgNPs synthesized in surfactant modified CCH shows the smaller size and narrower particle size distribution than in the unmodified CCH. This may be due to aggregates remains in existence in the AgNPs prepared in the CCH without surfactant inside. A noticeable result obtained in the CCH-R that shows a significantly high relative frequency in the 5 to 10 nm range indicates a more uniform particle size.

### 3.4. Deformability

The mechanical properties of materials can be used as a basis for consideration in describing the strength of the material. Deformability

in units of mm/g s indicates the level of depth of the needle that squeezes CCH (mm) by the load (g) loaded per second. The higher the strength of the hydrogel, the lower the deformability value. The CCH deformability results in Fig. 8a shows that loading AgNPs causes a decrease in deformability. This indicates that the presence of AgNPs can strengthen hydrogels. Ye et al. also obtained similar results, where the compressive stress of cellulose composite hydrogel was found to increase with the addition of AgNPs [66]. A similar phenomenon was also observed in surfactant-modified CCH, where the presence of AgNPs also helped reduce the level of deformability (Fig. S4).

The addition of surfactants, in contrast, exerts an effect on increasing deformability (decreased hydrogel strength). This can be attributed to the presence of surfactant micelles that act as lubricants in the hydrogel matrix. The presence of surfactant micelles in hydrogels

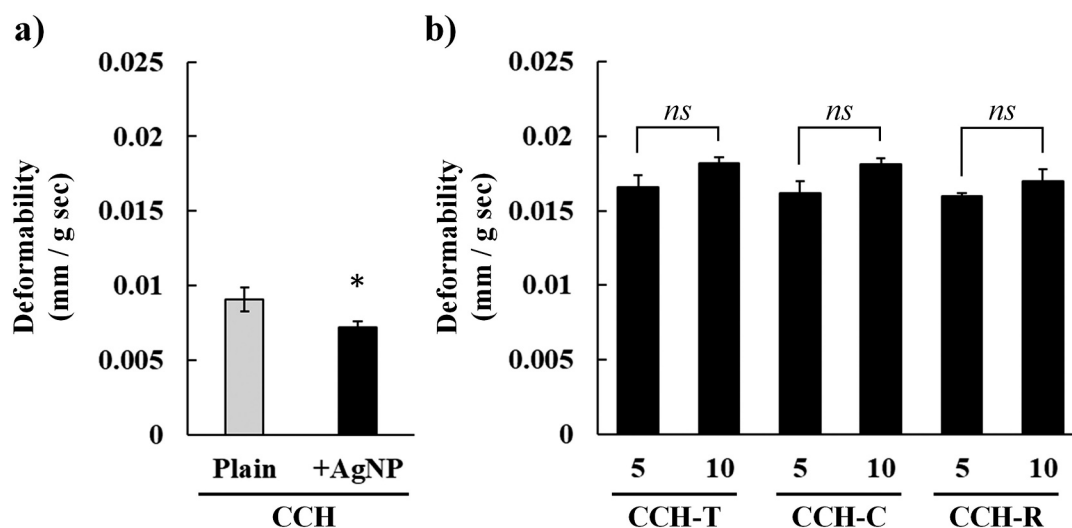


Fig. 8. Deformability of the prepared hydrogels without (gray bar) and with AgNPs loading (black bar). Data are mean  $\pm$  SD from 3 replications. The asterisks indicate the statistical significance examined by the Student's *t*-test; (\*, *P* value < 0.05; ns, not significant)—All data show uncertainty < 5%.

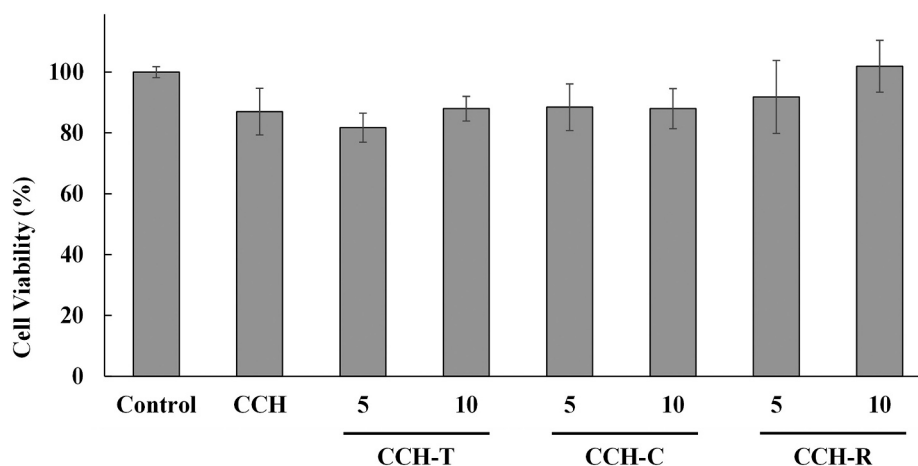


Fig. 9. Cell viability of the prepared hydrogels with AgNPs loading for 1-day incubation. All data show uncertainty < 5%.

results in reduced interaction between hydrogel molecules, and thus, reducing the strength of hydrogels [67]. The higher concentration of modifying surfactants gives a slight increase in deformability values, as shown in Fig. 8b.

### 3.5. Cell cytotoxicity

The cytotoxicity evaluation is an extensive way of demonstrating the biocompatibility of the prepared hydrogel as a wound dressing material. Fig. 9 shows that none of the remaining cell viability was lower than 80%. According to ISO 10993-5: 1999, no cytotoxic potential in samples with cell viability higher than 70%. Therefore, it can be concluded that the AgNPs loaded hydrogels can maintain the normal function of skin fibroblasts. It can also be noted that the use of surfactant higher than CMC did not exhibit toxicity even in the high concentration of 10 mM.

### 3.6. Antibacterial activities

The antibacterial activity of the sample was observed against gram-positive and gram-negative bacteria. The antibacterial activity is depicted from the presence of the zone of inhibition (ZOI), as shown in Fig. 10, the ZOI values are recorded in Table 2. The higher antibacterial activity is indicated by larger ZOI diameter, where the clear zones

around hydrogel discs indicate that hydrogels can inhibit bacterial growth [68]. The antibacterial mechanism of AgNPs has been reported in many studies [69,70]. Briefly, Ag, which is a soft acid, tends to interact with soft bases, here, sulfur contained in protein membranes and phosphorus in bacterial DNA. Since soft acid-soft base interaction is preferable than the interaction of AgNPs with the hydroxyl groups of cellulose hydrogel, thus AgNPs will be released from the hydrogel. This released AgNP then damages bacterial cells by inducing the formation of hydroxyl radicals and penetrate into/interferes with DNA replication through the damaged cells, and thereby causing cell death. The more AgNPs come into contact, the damaging effect to the bacterial cells will be exaggerated. From the results of ZOI measurements, it was found that CCH-C had the highest antibacterial activity, followed by CCH-R > CCH-T > CCH. This is because the presence of surfactants helps increase the loading of AgNPs so that antimicrobial activity also increases. Distinct to other systems, in CCH-C—Since CTAB itself possess an antibacterial activity (as observed in negative control); thus the antibacterial activity does not solely depend on the amount of AgNPs in its matrix but also due to the presence of CTAB. The presence of surfactants also helps prevent AgNPs aggregation, thereby increasing the dispersibility of AgNPs. This increases contact between AgNPs and bacteria, thereby increasing antibacterial activity [71].

As described in most studies [72–76], hydrogels containing AgNP have a better inhibitory effect on the growth of *E. coli* than *S. aureus*.

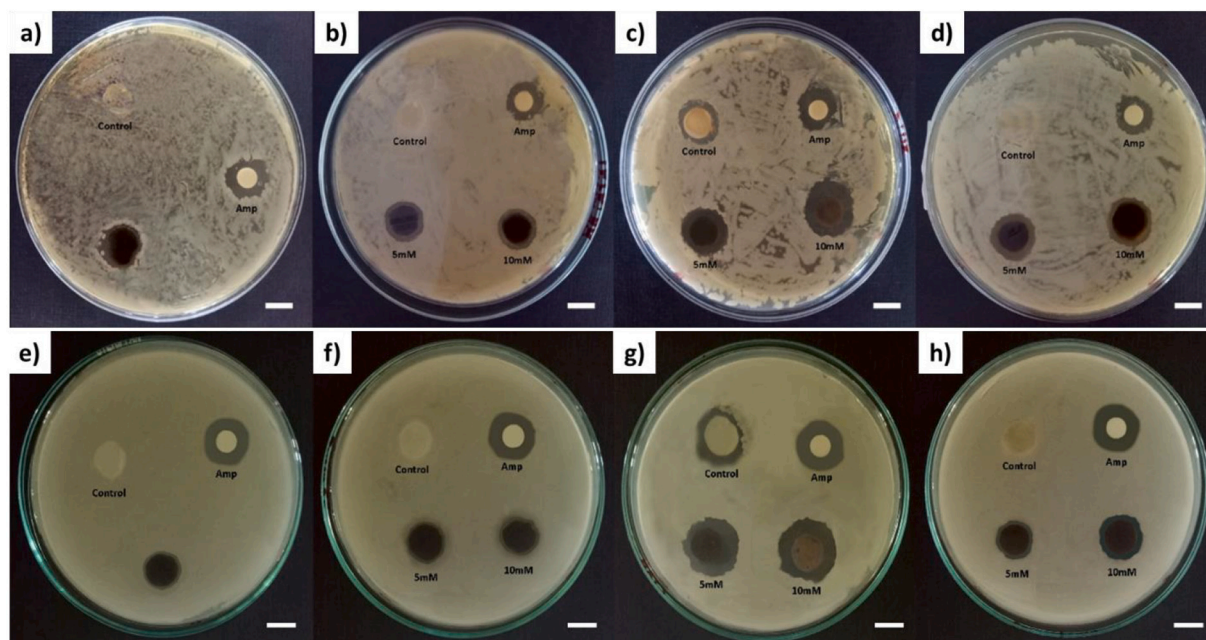


**Fig. 10.** Antimicrobial activity of AgNP-loaded (a) CCH (b) CCH-T (c) CCH-C (d) CCH-R against *E. coli*; (e) CCH (f) CCH-T (g) CCH-C (h) CCH-R against *S. aureus* after incubation for 24 h at 37 °C. Scale bars are 10 mm.

**Table 2**

Zone of inhibition (ZOI) of cellulose carbamate hydrogel (CCH) against *E. coli* and *S. aureus*.

Sample	Surfactant conc. (mM)	Amount of antibiotic or AgNP ( $\mu\text{g}$ )	ZOI (mm)	
			<i>E. coli</i>	<i>S. aureus</i>
Amp <sup>a</sup>	–	10.00	13.73 $\pm$ 0.76	15.42 $\pm$ 0.40
CCH	–	Control	0.00 $\pm$ 0.00	0.00 $\pm$ 0.00
	–	61.95	15.57 $\pm$ 0.50	12.62 $\pm$ 0.42
CCH-T	10	Control	0.00 $\pm$ 0.00	0.00 $\pm$ 0.00
	5	71.49	14.33 $\pm$ 0.28	13.17 $\pm$ 0.02
	10	75.30	14.57 $\pm$ 0.50	13.09 $\pm$ 0.30
CCH-C	10	Control	14.29 $\pm$ 0.31	16.05 $\pm$ 0.96
	5	84.80	16.91 $\pm$ 0.38	18.73 $\pm$ 0.42
	10	99.40	18.98 $\pm$ 0.42	19.84 $\pm$ 0.38
CCH-R	10	Control	0.00 $\pm$ 0.00	0.00 $\pm$ 0.00
	5	84.33	16.45 $\pm$ 0.25	12.54 $\pm$ 0.12
	10	101.50	16.87 $\pm$ 0.42	14.37 $\pm$ 0.35

<sup>a</sup> Amp was denoted ampicillin, the reference antibiotic used in this study.

AgNPs can easily penetrate the polysaccharide layer of *E. coli*, plus the thin peptidoglycan layer of *E. coli* (gram-negative) causes AgNPs to enter bacterial tissue easily [3,77]. In contrast, CCH-C showed better antimicrobial activity against *S. aureus* compared to *E. coli*. This result is in good agreement with previous studies conducted by Wieczorek et al., where CTAB showed higher antimicrobial activity against gram-positive bacteria than gram-negative bacteria [78]. Thus, CCH-C inhibition is dominated by CTAB rather than AgNPs.

Comparative studies of the antimicrobial effects of AgNPs and AgNPs-hybrid materials are summarized in Table S2. As shown from the ZOI value, AgNPs@CCH-R (in this work) showed better antimicrobial activity compared to AgNPs-hybrid carboxymethyl cellulose hydrogels [79], PPEGMA-ran-PAA copolymer hydrogel [80], and bioreduced AgNPs [81]. However, the material prepared in this work has lower activity compared to AgNPs-hybrid polycaprolactone nanofibers [82]. Nevertheless, AgNPs@CCH, which are modified by surfactants, can easily and cheaply be prepared from sustainable raw materials.

#### 4. Conclusion

Wound dressing with significant antibacterial activity and low-cytotoxicity was successfully prepared by incorporating silver nanoparticles (AgNPs) on rarasaponin-modified cellulose carbamate hydrogel (CCH-R). Incorporation of AgNPs on CCH was done by means of adsorption approach of AgNO<sub>3</sub> on CCH-R, followed by in situ reductions using sodium borohydride. The synergetic bacteriostatic and antibacterial effect of carbamate, rarasaponin (a natural surfactant), and AgNPs generated a hydrogel material with superior antimicrobial activity against gram-negative bacteria (*E. coli*) and gram-positive bacteria (*S. aureus*) with high biocompatibility toward skin fibroblast, L929 cell. While these findings unlocked a new approach for AgNPs loading, a limitation may raise due to the variations of the adsorption capacity of each material.

#### CRediT authorship contribution statement

**V. Bundjaja:** Investigation, Data Curation, Formal Analysis, Writing – Original Draft. **S. P. Santoso, A. E. Angkawijaya:** Conceptualization, Investigation, Funding Acquisition, Writing – Review & Editing. **M. Yuliana, F. E. Soetaredjo:** Conceptualization, Resources. **S. Ismadji, Y.-H. Ju:** Supervision, Writing – Review & Editing. **A. Ayucitra, C. Gunarto, M.-H. Ho:** Data Curation, Resources.

#### Declaration of competing interest

The authors declare no conflict of interest.

#### Acknowledgment

This study was supported by the Ministry of Research, Technology and Higher Education through a Research Grant with contract number 130Q/WM01.5/N/2020. The authors are grateful to Dr. Yi-Fan Jiang (National Taiwan University) for his assistance in collecting TEM images and SAED patterns.

## Appendix A. Supplementary data

Supplementary data to this article can be found online at <https://doi.org/10.1016/j.msec.2020.111542>.

## References

- [1] C. Martin, W.L. Low, M.C.I.M. Amin, I. Radecka, P. Raj, K. Kenward, Current trends in the development of wound dressings, biomaterials and devices, *Pharm. Pat. Anal.* 2 (2013) 341–359, <https://doi.org/10.4155/ppa.13.18>.
- [2] I. Sondi, B. Salopek-Sondi, Silver nanoparticles as antimicrobial agent: a case study on *E. coli* as a model for gram-negative bacteria, *J. Colloid Interface Sci.* 275 (2004) 177–182, <https://doi.org/10.1016/j.jcis.2004.02.012>.
- [3] S.-H. Kim, H.-S. Lee, D.-S. Ryu, S.-J. Choi, D.-S. Lee, Antibacterial activity of silver nanoparticles against *Staphylococcus aureus* and *Escherichia coli*, *Korean J. Microbiol. Biotechnol.* 39 (2011) 77–85.
- [4] C. Rigo, L. Ferroni, I. Tocco, M. Roman, I. Munivrana, C. Gardin, W. Cairns, V. Vindigni, B. Azzena, C. Barbante, Active silver nanoparticles for wound healing, *Int. J. Mol. Sci.* 14 (2013) 4817–4840 (doi:10.3390%2Fijms14034817).
- [5] M. Rai, A. Yadav, A. Gade, Silver nanoparticles as a new generation of antimicrobials, *Biotechnol. Adv.* 27 (2009) 76–83, <https://doi.org/10.1016/j.biotechadv.2008.09.002>.
- [6] H.H. Lara, N.V. Ayala-Núñez, L.d.C.I. Turrent, C.R. Padilla, Bactericidal effect of silver nanoparticles against multidrug-resistant bacteria, *World J. Microbiol. Biotechnol.* 26 (2010) 615–621, <https://doi.org/10.1007/s11274-009-0211-3>.
- [7] M. Rai, S. Deshmukh, A. Ingle, A. Gade, Silver nanoparticles: the powerful nano-weapon against multidrug-resistant bacteria, *J. Appl. Microbiol.* 112 (2012) 841–852, <https://doi.org/10.1111/j.1365-2672.2012.05253.x>.
- [8] A.-C. Burdusel, O. Gherasim, A.M. Grumezescu, L. Mogoantă, A. Fica, E. Andronescu, Biomedical applications of silver nanoparticles: an up-to-date overview, *Nanomaterials* 8 (2018) 681, <https://doi.org/10.3390/nano8090681>.
- [9] K.C. Song, S.M. Lee, T.S. Park, B.S. Lee, Preparation of colloidal silver nanoparticles by chemical reduction method, *Korean J. Chem. Eng.* 26 (2009) 153–155, <https://doi.org/10.1007/s11814-009-0024-y>.
- [10] M.G. Guzmán, J. Dille, S. Godet, Synthesis of silver nanoparticles by chemical reduction method and their antibacterial activity, *Int. J. Chem. Biomol. Eng.* 2 (2009) 104–111.
- [11] A. Callegari, D. Tonti, M. Chergui, Photochemically grown silver nanoparticles with wavelength-controlled size and shape, *Nano Lett.* 3 (2003) 1565–1568, <https://doi.org/10.1021/nl034757a>.
- [12] Y. Zhang, F. Chen, J. Zhuang, Y. Tang, D. Wang, Y. Wang, A. Dong, N. Ren, Synthesis of silver nanoparticles via electrochemical reduction on compact zeolite film modified electrodes, *ChemComm* (2002) 2814–2815, <https://doi.org/10.1039/B208222E>.
- [13] J.-P. Abid, A. Wark, P.-F. Brevet, H. Girault, Preparation of silver nanoparticles in solution from a silver salt by laser irradiation, *ChemComm* (2002) 792–793, <https://doi.org/10.1039/B200272H>.
- [14] K. Bogle, S. Dhole, V. Bhoraskar, Silver nanoparticles: synthesis and size control by electron irradiation, *Nanotechnology* 17 (2006) 3204, <https://doi.org/10.1088/0957-4484/17/13/021>.
- [15] X. Sun, Y. Luo, Preparation and size control of silver nanoparticles by a thermal method, *Mater. Lett.* 59 (2005) 3847–3850, <https://doi.org/10.1016/j.matlet.2005.07.021>.
- [16] P. Mohanpuria, N.K. Rana, S.K. Yadav, Biosynthesis of nanoparticles: technological concepts and future applications, *J. Nanopart. Res.* 10 (2008) 507–517, <https://doi.org/10.1007/s11051-007-9275-x>.
- [17] H. Korbekandi, S. Iravani, S. Abbasi, Optimization of biological synthesis of silver nanoparticles using *Lactobacillus casei* subsp. *casei*, *J. Chem. Technol. Biotechnol.* 87 (2012) 932–937, <https://doi.org/10.1002/jctb.3702>.
- [18] W. Zhang, X. Qiao, J. Chen, Synthesis of nanosilver colloidal particles in water/oil microemulsion, *Colloids Surf. A Physicochem. Eng. Asp.* 299 (2007) 22–28, <https://doi.org/10.1016/j.colsurfa.2006.11.012>.
- [19] A. Šilekaitė, I. Prosyčėvas, J. Puišio, A. Juraitis, A. Guobienė, Analysis of silver nanoparticles produced by chemical reduction of silver salt solution, *Mater. Sci.* 12 (2006) 1392–1320.
- [20] A. Panáček, L. Kvítek, M. Směkalová, R. Večeřová, M. Kolář, M. Röderová, F. Dyčka, M. Šebela, R. Prucek, O. Tomanec, Bacterial resistance to silver nanoparticles and how to overcome it, *Nat. Nanotechnol.* 13 (2018) 65, <https://doi.org/10.1038/s41565-017-0013-y>.
- [21] S. Magana, P. Quintana, D. Aguilar, J. Toledo, C. Angeles-Chavez, M. Cortes, L. Leon, Y. Freile-Pelegrín, T. Lopez, R.T. Sánchez, Antibacterial activity of montmorillonites modified with silver, *J. Mol. Catal. A Chem.* 281 (2008) 192–199, <https://doi.org/10.1016/j.molcata.2007.10.024>.
- [22] K. Shamel, M.B. Ahmad, M. Zargar, W.M.Z.W. Yunus, A. Rustaiyan, N.A. Ibrahim, Synthesis of silver nanoparticles in montmorillonite and their antibacterial behavior, *Int. J. J. 6* (2011) 581 (doi:10.2147%2FIJN.S17112).
- [23] K. Malachová, P. Praus, Z. Pavličková, M. Turicová, Activity of antibacterial compounds immobilised on montmorillonite, *Appl. Clay Sci.* 43 (2009) 364–368, <https://doi.org/10.1016/j.clay.2008.11.003>.
- [24] D. Jiraroj, S. Tungasmita, D.N. Tungasmita, Silver ions and silver nanoparticles in zeolite a composites for antibacterial activity, *Powder Technol.* 264 (2014) 418–422, <https://doi.org/10.1016/j.powtec.2014.05.049>.
- [25] S.C. Motshekga, S.S. Ray, M.S. Onyango, M.N. Momba, Microwave-assisted synthesis, characterization and antibacterial activity of Ag/ZnO nanoparticles supported bentonite clay, *J. Hazard. Mater.* 262 (2013) 439–446, <https://doi.org/10.1016/j.jhazmat.2013.08.074>.
- [26] L. Ai, J. Jiang, Catalytic reduction of 4-nitrophenol by silver nanoparticles stabilized on environmentally benign macroscopic biopolymer hydrogel, *Bioresour. Technol.* 132 (2013) 374–377, <https://doi.org/10.1016/j.biortech.2012.10.161>.
- [27] M. Yadollahi, S. Farhoudian, H. Namazi, One-pot synthesis of antibacterial chitosan/silver bio-nanocomposite hydrogel beads as drug delivery systems, *Int. J. Biol. Macromol.* 79 (2015) 37–43, <https://doi.org/10.1016/j.ijbiomac.2015.04.032>.
- [28] J. Cai, S. Kimura, M. Wada, S. Kuga, Nanoporous cellulose as metal nanoparticles support, *Biomacromolecules* 10 (2008) 87–94, <https://doi.org/10.1021/bm800919e>.
- [29] E.I. Alarcón, K.I. Udekwa, C.W. Noel, L.B.-P. Gagnon, P.K. Taylor, B. Vulesevic, M.J. Simpson, S. Gkotsis, M.M. Islam, C.-J. Lee, Safety and efficacy of composite collagen–silver nanoparticle hydrogels as tissue engineering scaffolds, *Nanoscale* 7 (2015) 18789–18798, <https://doi.org/10.1039/C5NR03826J>.
- [30] H. Yu, X. Xu, X. Chen, T. Lu, P. Zhang, X. Jing, Preparation and antibacterial effects of PVA-PVP hydrogels containing silver nanoparticles, *J. Appl. Polym. Sci.* 103 (2007) 125–133, <https://doi.org/10.1002/app.24835>.
- [31] C.M. González-Henríquez, G.d.C. Pizarro, M.A. Sarabia-Vallejos, C.A. Terraza, Z.E. Lopez-Cabana, In situ-preparation and characterization of silver-hema/pegda hydrogel matrix nanocomposites: silver inclusion studies into hydrogel matrix, *Arab. J. Chem.* (2014), <https://doi.org/10.1016/j.arabjc.2014.11.012>.
- [32] C.K. Field, M.D. Kerstein, Overview of wound healing in a moist environment, *Am. J. Surg.* 167 (1994) S2–S6, [https://doi.org/10.1016/0002-9610\(94\)90002-7](https://doi.org/10.1016/0002-9610(94)90002-7).
- [33] A. Salomé Veiga, J.P. Schneider, Antimicrobial hydrogels for the treatment of infection, *J. Pept. Sci.* 100 (2013) 637–644 (doi:10.1002%2Fjpep.22412).
- [34] S.F. Kabir, P.P. Sikdar, B. Haque, M.R. Bhuiyan, A. Ali, M. Islam, Cellulose-based hydrogel materials: chemistry, properties and their prospective applications, *Prog. Biomater.* 7 (2018) 153–174, <https://doi.org/10.1007/s40204-018-0095-0>.
- [35] N. Peng, Y. Wang, Q. Ye, L. Liang, Y. An, Q. Li, C. Chang, Biocompatible cellulose-based superabsorbent hydrogels with antimicrobial activity, *Carbohydr. Polym.* 137 (2016) 59–64, <https://doi.org/10.1016/j.carbpol.2015.10.057>.
- [36] N.T. Laçin, Development of biodegradable antibacterial cellulose based hydrogel membranes for wound healing, *Int. J. Biol. Macromol.* 67 (2014) 22–27, <https://doi.org/10.1016/j.ijbiomac.2014.03.003>.
- [37] C. Chang, L. Zhang, Cellulose-based hydrogels: present status and application prospects, *Carbohydr. Polym.* 84 (2011) 40–53, <https://doi.org/10.1016/j.carbpol.2010.12.023>.
- [38] S. Paunonen, Strength and barrier enhancements of cellophane and cellulose derivative films: a review, *BioResources* 8 (2013) 3098–3121, <https://doi.org/10.15376/biores.8.2.3098-3121>.
- [39] S. Gan, S. Zakaria, C.H. Chia, R.S. Chen, A.V. Ellis, H. Kaco, Highly porous regenerated cellulose hydrogel and aerogel prepared from hydrothermal synthesized cellulose carbamate, *PLoS One* 12 (2017) e0173743, <https://doi.org/10.1371/journal.pone.0173743>.
- [40] R. Cuahtecintzi-Delint, M.A. Mendez-Rojas, E.R. Bandala, M.A. Quiroz, S. Recillas, J.L. Sanchez-Salas, Enhanced antibacterial activity of CeO<sub>2</sub> nanoparticles by surfactants, *Int. J. Chem. React. Eng.* 11 (2013) 781–785, <https://doi.org/10.1515/ijcre-2012-0055>.
- [41] R.G. Sibal, R.P. Jaimangal, P.M. Coutts, J.A. Elliott, Evaluating a surfactant-containing polymeric membrane foam wound dressing with glycerin in patients with chronic pilonidal sinus disease, *Adv. Skin Wound Care* 31 (2018) 298–305, <https://doi.org/10.1097/01.asw.0000534702.34915.90>.
- [42] L. Kvítek, A. Panáček, J. Soukupova, M. Kolář, R. Večeřová, R. Prucek, M. Holecova, R. Zbořil, Effect of surfactants and polymers on stability and antibacterial activity of silver nanoparticles (nps), *J. Phys. Chem. C* 112 (2008) 5825–5834, <https://doi.org/10.1021/jp711616v>.
- [43] X. Zheng, L. Zhu, A. Yan, X. Wang, Y. Xie, Controlling synthesis of silver nanowires and dendrites in mixed surfactant solutions, *J. Colloid Interface Sci.* 268 (2003) 357–361, <https://doi.org/10.1016/j.jcis.2003.09.021>.
- [44] A. Kurniawan, H. Sutiono, Y.-H. Ju, F.E. Soetaredjo, A. Ayucitra, A. Yudha, S. Ismadji, Utilization of rarasaponin natural surfactant for organo-bentonite preparation: application for methylene blue removal from aqueous effluent, *Microporous Mesoporous Mater.* 142 (2011) 184–193, <https://doi.org/10.1016/j.micromeso.2010.11.032>.
- [45] S. Agnihotri, S. Mukherji, S. Mukherji, Antimicrobial chitosan–PVA hydrogel as a nanoreactor and immobilizing matrix for silver nanoparticles, *Appl. Nanosci.* 2 (2012) 179–188, <https://doi.org/10.1007/s13204-012-0080-1>.
- [46] J. Órfão, A. Silva, J. Pereira, S. Barata, I. Fonseca, P. Faria, M. Pereira, Adsorption of a reactive dye on chemically modified activated carbons—influence of pH, J.

- Colloid Interface Sci. 296 (2006) 480–489, <https://doi.org/10.1016/j.jcis.2005.09.063>.
- [47] Y. Fu, G. Li, R. Wang, F. Zhang, M. Qin, Effect of the molecular structure of acylating agents on the regioselectivity of cellulosic hydroxyl groups in ionic liquid, *BioResources* 12 (2017) 992–1006, <https://doi.org/10.15376/biores.12.1.992-1006>.
- [48] L.T.T. Vo, B. Široká, A.P. Manian, T. Bechtold, Functionalisation of cellulosic substrates by a facile solventless method of introducing carbamate groups, *Carbohydr. Polym.* 82 (2010) 1191–1197, <https://doi.org/10.1016/j.carbpol.2010.06.052>.
- [49] Y. Teng, G. Yu, Y. Fu, C. Yin, The preparation and study of regenerated cellulose fibers by cellulose carbamate pathway, *Int. J. Biol. Macromol.* 107 (2018) 383–392, <https://doi.org/10.1016/j.ijbiomac.2017.09.006>.
- [50] B. Xiong, P. Zhao, K. Hu, L. Zhang, G. Cheng, Dissolution of cellulose in aqueous NaOH/urea solution: role of urea, *Cellulose* 21 (2014) 1183–1192, <https://doi.org/10.1007/s10570-014-0221-7>.
- [51] S.P. Santoso, A. Kurniawan, F.E. Soetaredjo, K.-C. Cheng, J.N. Putro, S. Ismadji, Y.-H. Ju, Eco-friendly cellulose–bentonite porous composite hydrogels for adsorptive removal of azo dye and soilless culture, *Cellulose* 26 (2019) 3339–3358, <https://doi.org/10.1007/s10570-019-02314-2>.
- [52] J. Zhou, C. Chang, R. Zhang, L. Zhang, Hydrogels prepared from unsubstituted cellulose in NaOH/urea aqueous solution, *Macromol. Biosci.* 7 (2007) 804–809, <https://doi.org/10.1002/mabi.200700007>.
- [53] C. Chang, B. Duan, J. Cai, L.J.E.p.j. Zhang, Superabsorbent hydrogels based on cellulose for smart swelling and controllable delivery, *Eur. Polym. J.* 46 (2010) 92–100, <https://doi.org/10.1016/j.eurpolymj.2009.04.033>.
- [54] C. Chang, M. He, J. Zhou, L.J.M. Zhang, Swelling behaviors of pH-and salt-responsive cellulose-based hydrogels, *Macromolecules* 44 (2011) 1642–1648, <https://doi.org/10.1021/ma102801f>.
- [55] A.-A.M. Nada, S. Kamel, M. El-Sakhawy, Thermal behaviour and infrared spectroscopy of cellulose carbamates, *Polym. Degrad. Stab.* 70 (2000) 347–355, [https://doi.org/10.1016/S0141-3910\(00\)00119-1](https://doi.org/10.1016/S0141-3910(00)00119-1).
- [56] B.L. Tardy, S. Yokota, M. Ago, W. Xiang, T. Kondo, R. Bordes, O.J. Rojas, Nanocellulose–surfactant interactions, *Curr. Opin. Colloid Interface Sci.* 29 (2017) 57–67, <https://doi.org/10.1016/j.cocis.2017.02.004>.
- [57] R.J. Farn, *Chemistry and Technology of Surfactants*, John Wiley & Sons, 2008, <https://doi.org/10.1002/9780470988596>.
- [58] L. Aleshina, A. Prusskii, A. Mikhailidi, N. Kotelnikova, X-ray diffraction study of cellulose powders and their hydrogels. Computer modeling of the atomic structure, *Fibre Chem.* 50 (2018) 166–175, <https://doi.org/10.1007/s10692-018-9954-7>.
- [59] R. Xiong, C. Lu, Y. Wang, Z. Zhou, X. Zhang, Nanofibrillated cellulose as the support and reductant for the facile synthesis of Fe<sub>3</sub>O<sub>4</sub>/Ag nanocomposites with catalytic and antibacterial activity, *J. Mater. Chem. A* 1 (2013) 14910–14918, <https://doi.org/10.1039/C3TA13314A>.
- [60] S.V.K.R. Kummari, M.R. Kummara, R.R. Palem, S.R. Nagellea, Y. Shchipunov, C.S.J.P.I. Ha, Chitosan–poly (aminopropyl/phenylsilsesquioxane) hybrid nanocomposite membranes for antibacterial and drug delivery applications, *Polym. Int.* 64 (2015) 293–302, <https://doi.org/10.1002/pi.4789>.
- [61] X. Li, J. Shen, A. Du, Z. Zhang, G. Gao, H. Yang, J. Wu, Facile synthesis of silver nanoparticles with high concentration via a CTAB-induced silver mirror reaction, *Colloids Surf. A Physicochem. Eng. Asp.* 400 (2012) 73–79, <https://doi.org/10.1016/j.colsurfa.2012.03.002>.
- [62] X.-H. Liu, X.-H. Luo, S.-X. Lu, J.-C. Zhang, W.-L. Cao, A novel cetyltrimethyl ammonium silver bromide complex and silver bromide nanoparticles obtained by the surfactant counterion, *J. Colloid Interface Sci.* 307 (2007) 94–100, <https://doi.org/10.1016/j.jcis.2006.11.051>.
- [63] Y.M. Mohan, K. Lee, T. Premkumar, K.E. Geckeler, Hydrogel networks as nanoreactors: a novel approach to silver nanoparticles for antibacterial applications, *Polymer* 48 (2007) 158–164, <https://doi.org/10.1016/j.polymer.2006.10.045>.
- [64] L. Rhein, Surfactant action on skin and hair: Cleansing and skin reactivity mechanisms, in: I. Johansson, P. Somasundaran (Eds.), *Handbook for Cleaning/Decontamination of Surfaces*, Elsevier B.V., The Netherlands, 2007, p. 992, <https://doi.org/10.1016/B978-044451664-0/50009-7>.
- [65] C. Zhu, J. Xue, J. He, Controlled in-situ synthesis of silver nanoparticles in natural cellulose fibers toward highly efficient antimicrobial materials, *J. Nanosci. Nanotechnol.* 9 (2009) 3067–3074, <https://doi.org/10.1166/jnn.2009.212>.
- [66] D. Ye, Z. Zhong, H. Xu, C. Chang, Z. Yang, Y. Wang, Q. Ye, L. Zhang, Construction of cellulose/nanosilver sponge materials and their antibacterial activities for infected wounds healing, *Cellulose* 23 (2016) 749–763, <https://doi.org/10.1007/s10570-015-0851-4>.
- [67] Y. Wu, T. Tang, B. Bai, X. Tang, J. Wang, Y. Liu, An experimental study of interaction between surfactant and particle hydrogels, *Polymer* 52 (2011) 452–460, <https://doi.org/10.1016/j.polymer.2010.12.003>.
- [68] B. Bonev, J. Hooper, J. Parisot, Principles of assessing bacterial susceptibility to antibiotics using the agar diffusion method, *J. Antimicrob. Chemother.* 61 (2008) 1295–1301, <https://doi.org/10.1093/jac/dkn090>.
- [69] S. Prabhu, E.K. Poulouse, Silver nanoparticles: mechanism of antimicrobial action, synthesis, medical applications, and toxicity effects, *Int. Nano Lett.* 2 (2012) 32, <https://doi.org/10.1186/2228-5326-2-32>.
- [70] J.R. Morones, J.L. Elechiguerra, A. Camacho, K. Holt, J.B. Kouri, J.T. Ramirez, M.J. Yacaman, The bactericidal effect of silver nanoparticles, *Nanotechnology* 16 (2005) 2346, <https://doi.org/10.1088/0957-4484/16/10/059>.
- [71] S. Pal, Y.K. Tak, J.M. Song, Does the antibacterial activity of silver nanoparticles depend on the shape of the nanoparticle? A study of the gram-negative bacterium *Escherichia coli*, *Appl. Environ. Microbiol.* 73 (2007) 1712–1720, <https://doi.org/10.1128/aem.02218-06>.
- [72] N.H. Aldujaili, M.M. Alrufa, F.H. Sahib, Antibiofilm antibacterial and antioxidant activity of biosynthesized silver nanoparticles using pantoea agglomerans, *J. Pharm. Sci. Res.* 9 (2017) 1220.
- [73] S. Egger, R.P. Lehmann, M.J. Height, M.J. Loessner, M. Schuppler, Antimicrobial properties of a novel silver–silica nanocomposite material, *Appl. Environ. Microbiol.* 75 (2009) 2973–2976, <https://doi.org/10.1128/AEM.01658-08>.
- [74] S. Shrivastava, T. Bera, A. Roy, G. Singh, P. Ramachandrarao, D. Dash, Characterization of enhanced antibacterial effects of novel silver nanoparticles, *Nanotechnology* 18 (2007) 225103, <https://doi.org/10.1088/0957-4484/18/22/225103>.
- [75] K. Madhusudana Rao, K. Krishna Rao, G. Ramanjaneyulu, K. Chowdaji Rao, M. Subha, C.S. Ha, Biodegradable sodium alginate-based semi-interpenetrating polymer network hydrogels for antibacterial application, *J. Biomed. Mater. Res. A* 102 (2014) 3196–3206, <https://doi.org/10.1002/jbm.a.34991>.
- [76] K.M. Rao, A. Kumar, A. Haider, S.S. Han, Polysaccharides based antibacterial polyelectrolyte hydrogels with silver nanoparticles, *Mater. Lett.* 184 (2016) 189–192, <https://doi.org/10.1016/j.matlet.2016.08.043>.
- [77] S. Mohanbaba, S. Gurunathan, Differential biological activities of silver nanoparticles against gram-negative and gram-positive bacteria: a novel approach for antimicrobial therapy, *Nanobiomaterials in Antimicrobial Therapy*, Elsevier, 2016, pp. 193–227, <https://doi.org/10.1016/B978-0-323-42864-4.00006-3>.
- [78] D. Wiczorek, D. Gwiazdowska, K. Michocka, D. Kwaśniewska, K. Kluczyńska, Antibacterial activity of selected surfactants, *Polish J. Commodity Sci.* 2 (2014) 142–149.
- [79] A. Hebeish, M. Hashem, M.A. El-Hady, S. Sharaf, Development of cmc hydrogels loaded with silver nanoparticles for medical applications, *Carbohydr. Polym.* 92 (2013) 407–413, <https://doi.org/10.1016/j.carbpol.2012.08.094>.
- [80] Y. Niu, T. Guo, X. Yuan, Y. Zhao, L. Ren, An injectable supramolecular hydrogel hybridized with silver nanoparticles for antibacterial application, *Soft Matter* 14 (2018) 1227–1234, <https://doi.org/10.1039/C7SM02251D>.
- [81] A.R. Shahverdi, A. Fakhimi, H.R. Shahverdi, S. Minaian, Synthesis and effect of silver nanoparticles on the antibacterial activity of different antibiotics against *staphylococcus aureus* and *escherichia coli*, *Nanomed. Nanotechnol. Biol. Med.* 3 (2007) 168–171, <https://doi.org/10.1016/j.nano.2007.02.001>.
- [82] J. López-Esparza, L.n.F. Espinosa-Cristóbal, A. Donohue-Cornejo, S.n.Y. Reyes-López, Antimicrobial activity of silver nanoparticles in polycaprolactone nanofibers against gram-positive and gram-negative bacteria, *Ind. Eng. Chem. Res.* 55 (2016) 12532–12538, <https://doi.org/10.1021/acs.iecr.6b02300>.

**Vania Bundjaja** is a Master student in the Department of Chemical Engineering, National Taiwan University of Science and Technology. She has outstanding track record in research and publications. Her research works include material design for adsorption and drug delivery systems.



**Sheila Permatasari Santoso** is currently working as a lecturer and researcher at Department of Chemical Engineering, Widya Mandala Surabaya Catholic University. She obtained her PhD degree (2016) from National Taiwan University of Science and Technology. Her research interests include hybrid materials for environmental and biotechnology application.



**Artik Elisa Angkawijaya** is a Project Assistant Professor in the Graduate Institute of Applied Science and Technology, National Taiwan University of Science and Technology. Her research interest span from plant metabolic adaptation to utilization of phytochemicals and under-utilized biomass for biosorbent preparation.





**Maria Yuliana** is currently working as a lecturer and researcher at Department of Chemical Engineering, Widya Mandala Surabaya Catholic University. She obtained her PhD degree (2012) from National Taiwan University of Science and Technology. Her expertise includes waste-to-energy and catalyst design.



**Chintya Gunarto** is a Doctoral student in the Department of Chemical Engineering, National Taiwan University of Science and Technology. She has outstanding track record in research and publications. Her research works include adsorption and drug delivery system.



**Felycia Edi Soetaredjo** is a Professor and senior researcher at the Department of Chemical Engineering, Widya Mandala Surabaya Catholic University. She obtained her PhD degree (2013) from National Taiwan University of Science and Technology. Her research interests include material designs for water and wastewater treatment.



**Yi-Hsu Ju**, a Project Professor in the Graduate Institute of Applied Science and Technology, National Taiwan University of Science and Technology, has his research interests in the areas of Bio-chemical engineering, Bioenergy, Isolation and Identification of bio-active compounds.



**Suryadi Ismadji** is a professor at Department of Chemical Engineering, Widya Mandala Surabaya Catholic University. He obtained his PhD degree (2002) from The University of Queensland, Australia. His research interests include the development of composite material for adsorption, catalyst, and drug-delivery systems.



**Ming-Hua Ho** is a professor at Department of Chemical Engineering, National Taiwan University of Science and Technology. She obtained her PhD degree (2004) from National Taiwan University. Her research interests include biomaterials, biocompatibility analysis and tissue engineering.



**Aning Ayucitra** is currently working as a lecturer and researcher at Department of Chemical Engineering, Widya Mandala Surabaya Catholic University. She obtained her PhD degree (2020) from National Taiwan University of Science and Technology. Her research works include material design for adsorption and drug delivery systems.